substantial capital investments. Even if the increasing OPEC market share leads to significantly higher prices, capital markets may not judge the price increases to be sufficiently robust or stable for development of substitutes on a large scale.


REFERENCES AND NOTES

1. J. F. Bookout, paper presented at the 28th International Geologic Congress, Washington, DC, 10 July 1989.
2. C. D. Masters, D. H. Root, E. D. Attanasi, *Annu. Rev. Energy* **15**, 23 (1990).
3. C. D. Masters, E. D. Attanasi, W. D. Dietzman, R. F. Meyer, D. H. Root, in *Proceedings of the 12th World Petroleum Congress* (Wiley, Chichester, 1987), vol. 5, pp. 3–27.
4. G. F. Ulmishek and H. D. Klemme, *U.S. Geol. Surv. Bull. 1931* (1990).
5. A. M. Ziegler, C. R. Scotese, S. F. Barrett, in *Tidal Friction and the Earth's Rotation II*, P. Brosche and J. Sunderman, Eds. (Springer-Verlag, Berlin, 1982), pp. 240–252.
6. See Masters *et al.* (*2*) for a more extensive listing by country.
7. *Reserves of Crude Oil, Natural Gas Liquids, and Natural Gas in the United States and Canada as of December 31*, annual volumes from 1966 through 1979 (American Petroleum Institute, Washington, DC), vols. 21–34.
8. *Energy Information Administration Report DOE/EIA-0534* (U.S. Department of Energy, Washington, DC, 1990).
9. *World Oil* **209** (no. 2), 30 (1989).
10. D. H. Root, *U.S. Geol. Surv. Circ. 860* (1981).
11. _____, E. D. Attanasi, C. D. Masters, *U.S. Geol. Surv. Open-File Rep. 90-280* (1990).
12. *Enhanced Oil Recovery* (National Petroleum Council, Washington, DC, 1984).
13. G. J. Fiorillo, in *Exploration for Heavy Crude Oil and Natural Bitumen*, vol. 25 of *Studies in Geology*, R. F. Meyer, Ed. (American Association of Petroleum Geologists, Los Angeles, 1987), pp. 103–114.
14. R. A. Corbett, *Oil Gas J.* **87**, 33 (1989).
15. *Pet. Intell. Wkly.* **28** (suppl.) (no. 46) (13 November 1989).
16. *Fuels to Drive Our Future* (National Research Council, Washington, DC, 1990).
17. *Launch of Shell MDS Project* (News release, Shell Malaysia, Kuala Lumpur, Malaysia, 22 August 1989).
18. R. F. Mast *et al.*, *Estimates of Undiscovered Conventional Oil and Gas Resources in the United States—a Part of the Nation's Energy Endowment* (U.S. Geological Survey and Minerals Management Service, Washington, DC, 1989).
19. *Twentieth Century Petroleum Statistics* (DeGolyer & McNaughton, Dallas, 1988).
20. *World Oil* **132**, 58 (1951).
21. *British Petroleum Review of World Gas* (British Petroleum Company, London, 1989).
22. *World Energy Supplies 1950–1974*, United Nations Statistical Paper Series J, no. 19 (United Nations, New York, 1976).


23. Background information essential to the preparation of this article was developed in concert with our colleagues in the World Energy Resources Program of the U.S. Geological Survey and the Foreign Energy Supply Assessment Program of Energy Information Administration of the Department of Energy. Basic petroleum data derive primarily from Petroconsultants S.A.


# Advances in Helioseismology


K. G. LIBBRECHT AND M. F. WOODARD



**Globally coherent oscillation modes were discovered in the sun about a decade ago, providing a unique seismological probe of the solar interior. Current observations detect modes that are phase-coherent for up to 1 year, with surface velocity amplitudes as low as 2 millimeters per second, and thousands of mode frequencies have been measured to accuracies as high as 1 part in $10^5$. This article discusses the properties of these oscillation modes and the ways in which they are adding to our understanding of the structure and dynamics of the sun.**


HELIOSEISMOLOGY, THE STUDY OF SOLAR OSCILLATIONS and their use as a probe of the sun's interior, is still a relatively young field. High-degree solar oscillations were first observed in the early 1960s (*1, 2*), and it was just over a decade ago that globally coherent oscillation modes were observed in the sun (*3*). In this short amount of time, however, the quality of the observations has improved greatly, and there have been substantial advances in our theoretical understanding of these oscillations [see the review articles on helioseismology (*4*)]. The observations have allowed us to accurately measure the depth of the solar convection zone as well as the sun's internal rotation profile, and to infer the temperature of the solar core (important for unraveling the solar neutrino problem).

Starting with a model for the overall structure of the sun, one can show with linear adiabatic perturbation theory that small-amplitude oscillations of the model about its equilibrium state can be classified into three types (*4*): (i) p-modes, which have pressure as the dominant restoring force; (ii) g-modes, for which gravity, or buoyancy, is the primary restoring force; and (iii) f-modes, which are nearly compressionless surface waves. Our discussion here will focus on p- and f-modes, for which there is clear and abundant observational data. g-Modes, according to calculation, are predominantly trapped deep in the solar interior, and it seems likely that these modes are not excited to observable amplitudes at the sun's surface. Some possible g-mode detections have been reported, but the observations at this point are still not convincing.

p-Modes are essentially acoustic (sound) waves propagating through the solar interior. For frequencies below a maximum acoustic cutoff frequency, $\nu < \nu_{a,\,max} \approx 5.3$ mHz, acoustic waves in the interior are reflected near the solar surface, forming an acoustic cavity inside the sun (*4*); for $\nu > \nu_{a,\,max}$, waves propagate through the surface and their energy is quickly dissipated. Because the wave damping is small inside the sun, interference organizes the reflected waves into the normal modes of the acoustic cavity, which are the p-modes. For our discussion these modes can be thought of as a set of harmonic oscillators, each uncoupled to all the rest, independently interacting with weak driving and damping forces. [Nonlinear coupling between modes has been found theoretically to be quite small (*5*).]

The perturbation of a scalar quantity in the solar interior, such as pressure $p$, resulting from an oscillation mode, can be written as an eigenfunction

$$\delta p(\mathbf{r},t) = \mathrm{Re}[\delta p_{n\ell}(r) Y_\ell^m(\theta,\phi) \exp(i2\pi\nu_{n\ell m} t)] \quad (1)$$

with frequency eigenvalue $\nu_{n\ell m}$, where $Y_\ell^m(\theta,\phi)$ is a spherical harmonic. Each mode is labeled with three integer "quantum"


K. G. Libbrecht is in the Department of Astrophysics and M. F. Woodard is a senior research fellow at California Institute of Technology, Mail Stop 264-33, Pasadena, CA 91125.

numbers $n$, $\ell$, and $m$; $n$ counts the number of radial nodes in the wavefunction, and $\ell$ and $m$ describe the nodes in $\theta$ and $\phi$. Sample radial wavefunctions have been plotted by several investigators (*4*). Figure 1 shows some p-mode frequencies measured by Libbrecht *et al.* as a function of degree $\ell$ (*6*). Note the very high accuracy of the observed frequencies, possible because the modes have measured quality factors as high as $Q \approx 20{,}000$. The f-modes, which have no radial nodes, can be thought of as an extension of the p-modes, forming another lower frequency ridge with $n = 0$. Although f-modes have not yet been observed at the $\ell$ values shown in Fig. 1, they are frequently observed at higher $\ell$, where their surface amplitudes are greater.

In order to understand some of the observed trends in the p-mode data, one must be aware of the basic properties of the mode eigenfunctions, particularly near the upper and lower reflection points. Close to the upper reflection point, always near the solar surface, the vertical wavelength of the eigenfunction is much smaller than the horizontal wavelength (for $\ell \ll 1000$). Thus the structure of the eigenfunction is nearly $\ell$-independent near the surface. On the other hand, an acoustic wave ceases to propagate once the frequency is below the acoustic cutoff frequency, that is, $\nu < \nu_a \simeq c/4\pi H$, where $c$ is the speed of sound and $H$ is the atmospheric scale height. Because $c/H \propto T^{-1/2}$, and temperature $T$ increases rapidly with depth below the solar surface, we find that low-frequency modes are trapped farther below the solar surface than higher frequency modes. Above the upper reflection point the remaining solar atmosphere oscillates up and down like a rigid body. The structure of the $p$-mode eigenfunctions near the solar surface, which in general depends on $n$ and $\ell$, is to first order dependent only on $\nu_{n\ell}$.

The lower reflection point $r_t$, deep in the solar interior, is given by $c(r_t)/r_t \simeq 2\pi\nu/L$, where $L^2 = \ell(\ell + 1)$, and thus depends on both $\nu$ and $\ell$; for fixed $\nu$, lower $\ell$ modes propagate deeper into the solar interior than those with higher $\ell$. At $\nu = 3$ mHz, near the peak in p-mode amplitudes, the reflection point is at the base of the convection zone, $r_t/R_\odot = 0.71$, for $\ell \approx 40$, where $R_\odot$ is the radius of the sun.

A particularly useful concept is that of the mode "mass," defined by $M = E/\langle\nu^2_{\text{surf}}\rangle$, where $E$ is the mode energy and $\langle\nu^2_{\text{surf}}\rangle$ is its mean squared surface velocity; typical mode masses are shown in Fig. 2. The mass increases sharply for $\nu < 2$ mHz because these lower frequency modes are trapped deeper inside the sun, leading to a smaller $\langle\nu^2_{\text{surf}}\rangle$ for a given $E$. Similarly, at constant $\nu$, a deeper lower reflection point (lower $\ell$) leads to a higher mode mass.

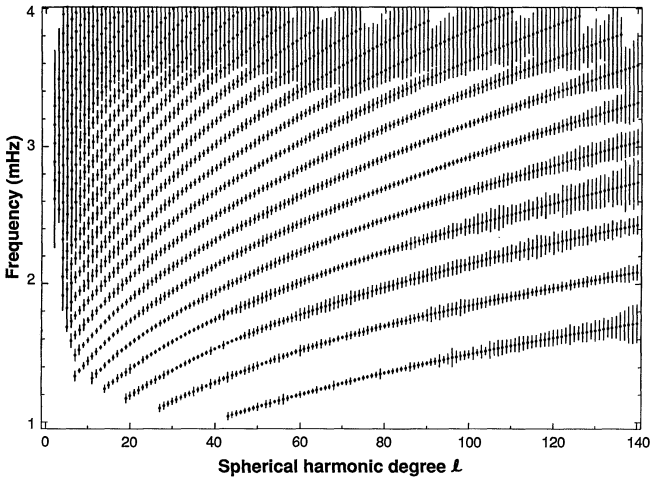


**Fig. 1.** Schematic plot showing p-mode frequencies measured by Libbrecht and Woodard in 1986 from Big Bear Solar Observatory, California Institute of Technology. The usual 1$\sigma$ error bars have been magnified by a factor of 1000 to make them visible. Each point shows a mode multiplet frequency $\bar{\nu}_{n\ell}$; the different ridges correspond to fixed values of radial order $n$ (equal to the number of radial nodes in the wavefunction), where the lowest frequency ridge has $n = 1$. [Adapted from (*15*)]

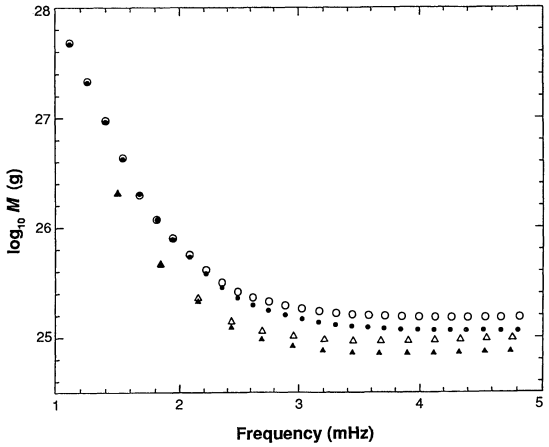


**Fig. 2.** Mode mass $M_{n\ell m}$, defined as the mode energy divided by its mean squared surface velocity. A range in $n$ is shown for $\ell = 0$ (circles) and $\ell = 100$ (triangles); the open characters use the surface velocity at $\tau_{5000} = 0.5$, and the filled characters are for $\tau_{5000} = 0.1$. For higher $\ell$, the mode mass at fixed frequency is roughly proportional to $\ell^{-1/2}$. [Adapted from (*24*)]

## Structure of the Solar Interior

By comparing measured p-mode frequencies with solar model calculations, we can in principle infer some properties of the solar interior; recent attempts to determine the solar helium abundance are a good example (*7*). In practice this process has been a difficult one, primarily because of the complexity of the physics that goes into the solar interior models. If we use state-of-the-art solar models, we find that the calculated frequencies match the measured frequencies to better than 1% (*4*), which is an indication of the overall accuracy of our current solar models. Of the remaining discrepancy, most can be shown to come from inaccuracies in the model near the solar surface (*8*); this is because the mode frequencies are most sensitive to the surface structure (because the sound speed is lowest there), while at the same time the surface layers are the most difficult to model accurately.

By comparing modes with different $\ell$ and $\nu$, we find that it is possible to peel away the surface uncertainties and infer in a roughly

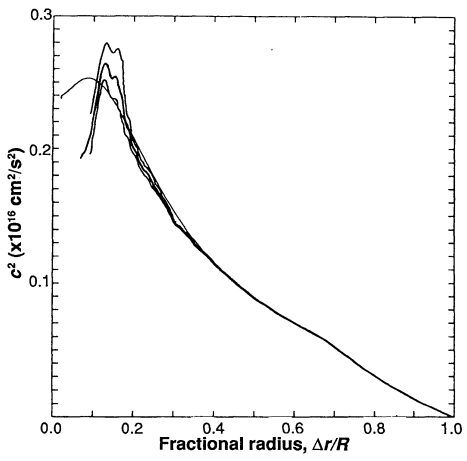


**Fig. 3.** The square of the sound speed inside the sun, as a function of fractional radius. The thick curve shows the inversion result from observational data, flanked by 1$\sigma$ confidence limits; the smooth thin curve shows the value of a theoretical solar model. The large discrepancy between the inversion and the model for $r/R_\odot < 0.2$ results mainly from the fact that the p-modes do not probe the deep interior very well. [Adapted from (*10*)]

model-independent way the sound speed as a function of depth deep inside the sun (*9–11*); Fig. 3 shows one example of such an inversion. The difference between inferred and model sound speeds, $\Delta c/c$, is less than 1 to 2% for $r/R_\odot > 0.2$, and the difference appears to be mostly dependent on the details of the solar model used, for instance, the detailed formulation of the equation of state for the solar plasma. Known uncertainties in the calculated opacity tables used to generate the solar models are sufficient to lead to $\Delta c/c$ values of this order.

Of particular interest is the structure of the deepest core of the sun, where nuclear burning and neutrino production are taking place. The sound speed inversions are most uncertain below $r/R_\odot = 0.2$ (Fig. 3); this is primarily because the p-modes are the most sensitive to surface structure and therefore do not probe the deep interior very well. Nevertheless, data from the lowest $\ell$ modes now indicate that standard solar models give a fairly accurate picture of the structure of the solar core, suggesting that neutrino physics, not solar physics, is the most likely explanation of the solar neutrino problem (*12*). Additional data and analysis are needed to confirm this result, however.

One spectacular success of the sound speed inversions is a very accurate determination of the depth of the convection zone (Fig. 4). Defining the base of the convection zone as that position $r_b$ where the temperature gradient makes a transition from subadiabatic to adiabatic, Christensen-Dalsgaard *et al.* (*13*) find $r_b/R_\odot = 0.713 \pm 0.003$, and $c(r_b) = 0.223 \pm 0.002$ Mm/s. Such an inference shows how a relatively simple bit of information can be extracted to high accuracy from a complex spectrum of p-mode frequencies.

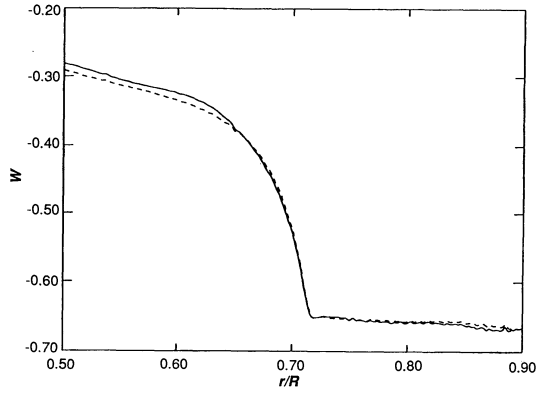


**Fig. 4.** The function $W = (r^2/GM_\odot)(dc^2/dr)$ as a function of fractional radius near the base of the convection zone, where $G$ is the gravitational constant and $M_\odot$ is the solar mass; in the convection zone we should have $W \simeq 1 - \gamma$, where $\gamma$ is the adiabatic index. The solid curve is from an inversion of solar data, and the dashed curve is from a reference model. The break at $r/R = 0.713$ shows the change in solar temperature gradient from nearly adiabatic inside the convection zone to subadiabatic below. [Adapted from (*13*)]

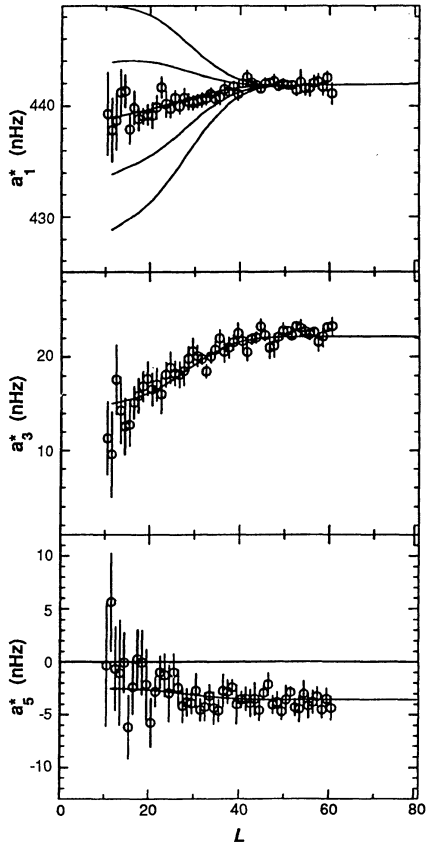


**Fig. 5.** p-Mode splitting data, where $a_i^*(\ell)$ represents the splitting coefficient $a_i$ ($\ell$, $n$) interpolated to a frequency of 2.5 mHz, together with splittings calculated from a family of solar rotation models. The models have surface-like rotation throughout the convection zone, $\Omega(r, \theta)/2\pi = 461 - 60\cos^2\theta - 75\cos^4\theta$ nHz for $r/R_\odot > 0.71$, where $\theta$ is solar colatitude, followed by solid-body rotation for $r/R_\odot < 0.71$. From bottom to top, the $a_1^*$ curves correspond to models with interior rotation rates from 404 to 468 nHz, in evenly spaced 16-nHz intervals. Models like this demonstrate that the radiative interior of the sun, at least for $r/R_\odot > 0.4$, cannot be rotating much faster than the surface rate. [Adapted from (*16*)]

## The Solar Rotation

Another area in which significant advances have been made recently is that of the p-mode frequency splittings, which have been used to determine the solar rotation rate through most of the solar interior. Because the sun is not spherically symmetric, the mode frequencies are not completely degenerate in $m$, and the frequencies $\nu_{n\ell m}$ in an ($n\ell$) multiplet are said to be split, analogous to the Zeeman splitting of degenerate atomic energy levels. Observers tend to fit the measured frequencies for each multiplet to a sum of Legendre polynomials in $m/L$:

$$\nu_{n\ell m} \rightarrow \bar{\nu}_{n\ell} + L \sum_{i=1} a_i P_i(m/L) \qquad (2)$$

where the $a_i$ have been measured to be significantly nonzero up to as high as $i = 12$ (*14*). In such an expansion, the odd-coefficient terms, $a_1$, $a_3$, $a_5$, and so forth, are nonzero because of the latitude- and depth-dependent solar rotation velocity; waves propagating along the equator in the direction of the solar rotation appear, to a fixed observer, to have a higher frequency than waves propagating in the opposite direction. The terms with even coefficients, however, are by symmetry insensitive to the solar rotation (a small but measurable $a_2$ does arise from the solar oblateness) and instead measure predominantly the latitude- and depth-dependent perturbation of the solar surface structure resulting from solar magnetic activity (*15*).

Figure 5 shows some recent measurements and indicates how the calculated $a_i$ depend on the assumed rotation profile inside the sun (*16*). Figure 6 shows an inversion of the data to determine the best-fit

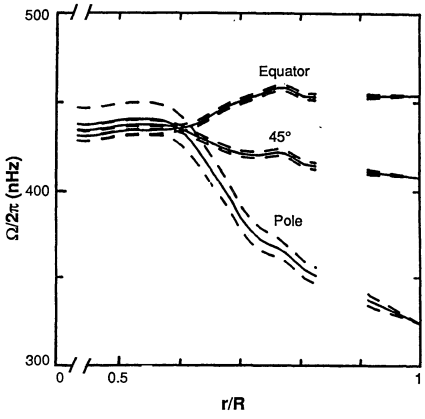


**Fig. 6.** Solar interior rotation profile, as inferred from an inversion of p-mode splitting data. The rotation rate depends on latitude but not radius throughout the convection zone, with a transition to solid-body rotation below. This inversion does not extend much above 0.8 $R_\odot$ or below 0.4 $R_\odot$; the observed surface rotation is indicated, but the rotation rate of the deep interior remains largely unknown. [Adapted from (*17*)]

rotation profile (*17*). These results reveal that the latitude-dependent rotation profile seen at the solar surface extends down through the convection zone; that is, the angular velocity is $\Omega(r, \theta) \approx \Omega(R_\odot, \theta)$ for $r/R_\odot > 0.7$, where $\theta$ is the solar colatitude, whereas in the radiative interior the rotation assumes a solid-body profile, $\Omega(r, \theta)/2\pi \approx 430$ nHz for $0.4 < r/R_\odot < 0.6$. Computer simulations of the solar convective zone suggest a qualitatively different picture of the sun's interior rotation in that region (*18*). At present there is no obvious theoretical explanation for the seismologically inferred rotation profile.

For $r/R_\odot < 0.4$ the existing data do not provide a clear picture. Solar model calculations including rotation suggest that a rapidly rotating core may be present (*19*); however, even a small magnetic field in the radiative interior would halt any such a differential rotation (*20*). Further data for the lowest $\ell$ values should decide this point in the not-too-distant future.

## Time-Dependent Mode Frequencies

p-Mode frequency measurements with accuracies like those in Fig. 1 have been measured for several years, allowing the detection of frequency shifts associated with the changing level of solar magnetic activity. Frequency shifts were first detected in low-$\ell$ data by Woodard and Noyes (*21*), and more recent observations show that the frequency shifts depend strongly on p-mode frequency [Fig. 7 (*15*)]. The more obvious trend in these data, that the high-$\nu$ modes experience a greater shift than low-$\nu$ modes, is understood as a time-dependent perturbation in the near-surface layers of the sun, presumably related to the surface magnetic fields associated with the solar magnetic cycle. Because the low-$\nu$ modes are trapped deeper below the surface, these modes do not "see" the perturbation as strongly and thus show a smaller frequency shift. The $\ell$ dependence of the frequency shift (Fig. 7B) is also consistent with this interpretation. Goldreich *et al.* (*22*) have found that a flux-tube model of the surface magnetic fields can fit these data quite well, provided that the magnetic field strength $B$ increases with depth approximately as $B^2 \sim \rho^{1/3}$, where $\rho$ is density, at least at shallow depths.

A particularly surprising aspect of the measurements (Fig. 7A) is that at the highest frequencies accurately measured, $\nu \simeq 4$ mHz, the frequency shift turns sharply down. Perhaps the most probable explanation for this behavior (*22*) involves a second acoustic cavity that is theoretically expected to be present in the solar chromosphere. Modes trapped in the solar interior can "tunnel" through the photosphere and interact with this chromospheric cavity; the greatest interaction would naturally be for modes with frequencies in resonance with the chromospheric cavity, $\nu \approx 4$ mHz. As the chromosphere changes with solar cycle, it affects the frequencies of modes that propagate in it. The sudden change in $\Delta\nu$ near $\nu \simeq 4$ mHz is explained by the fact that only modes very near resonance have large amplitudes in the chromosphere, so only these modes are significantly affected by the chromospheric changes.

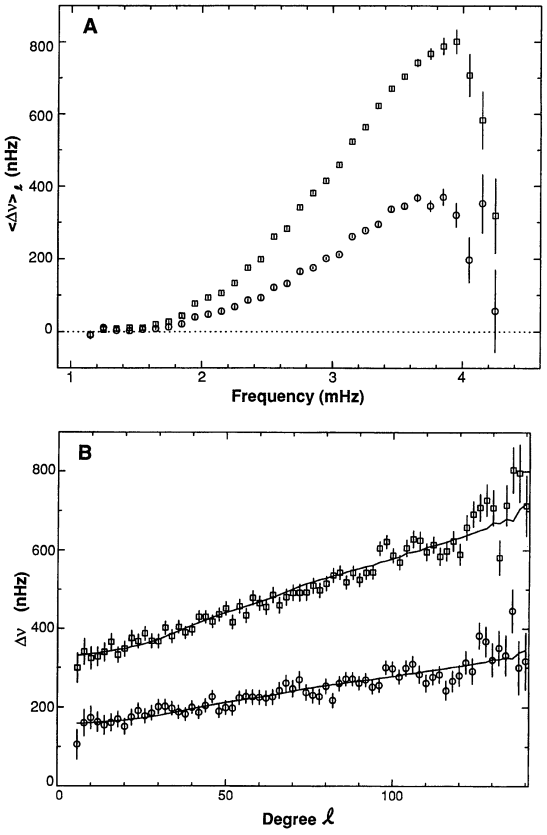


**Fig. 7.** p-Mode frequency changes with time. (**A**) Frequency differences $\nu_{1989} - \nu_{1986}$ (squares) and $\nu_{1988} - \nu_{1986}$ (circles) as a function of mode frequency $\nu$, averaged over degree with $4 \leq \ell \leq 140$. The solar minimum was in 1986, and the solar maximum was near 1989. (**B**) p-Mode frequency differences at $\nu = 3$ mHz, as a function of degree $\ell$. The solid lines show the inverse mode mass $M^{-1}(\nu = 3$ mHz, $\ell)$ scaled to fit the data (*15*).

## Excitation and Damping

Given a model of the structure of the sun, it is straightforward to calculate the various mode eigenfrequencies $\nu_{n\ell m}$, if we assume small-amplitude adiabatic oscillations. And, as we have discussed, the calculated frequencies are in excellent agreement with those measured, the remaining discrepancies being due mainly to surface uncertainties. It is a much more challenging task to calculate the expected mode amplitudes, because these depend in detail on the dynamics of the excitation and damping mechanisms, which cannot be approximated in an adiabatic limit. A solution to this problem will be welcomed by asteroseismologists, because an understanding of mode excitation in the sun should allow the prediction of acoustic mode amplitudes on other stars.

Figures 8 and 9 show the observed mode amplitudes (converted to average solar surface velocity per mode) and linewidths at low $\ell$ values. The lowest frequency modes observed have surface amplitudes of only a few millimeters per second and are phase-coherent for nearly 1 year. Kaufman (*23*) found that at higher $\ell$ the mode amplitudes first increase

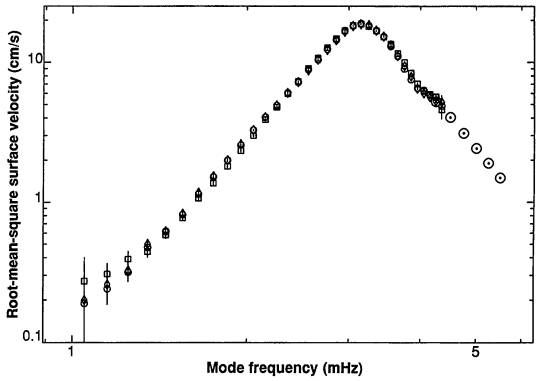


**Fig. 8.** Root-mean-square surface velocity per mode for low-$\ell$ p-modes. The data represent an average over $\ell$ values from 5 to 60, scaled to give the amplitude of $\ell = 0$ modes. Squares, circles, and diamonds show data from 1986, 1988, and 1989, respectively; the different years were scaled to match the 1986 measurements. The large circles at high frequency are from a separate analysis of $\ell = 60$ data (*34*). Between solar minimum (near 1986) and maximum (near 1989) the functional form of the p-mode amplitudes did not change significantly. The lowest frequency modes have surface amplitudes of only a few millimeters per second.

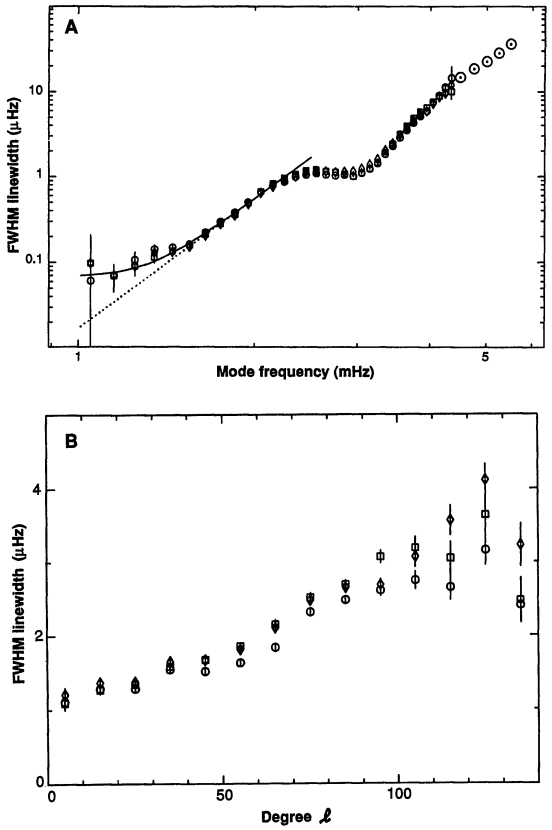


**Fig. 9.** (**A**) Full-width at half-maximum (FWHM) linewidths of low-$\ell$ solar p-modes, assuming Lorentzian line profiles; the notation is similar to that in Fig. 8. Here the different years of data were not independently scaled, but all were extrapolated [based on the results in (B)] to the expected $\ell = 0$ linewidths. The dotted line shows a power law behavior, with $\Gamma \sim \nu^5$; the solid line is the expected measured linewidth from this power law, with the finite time span of the observations (about 5 months) taken into account. The lowest frequency modes measured are probably phase-coherent for of order 1 year. (**B**) p-Mode linewidths averaged over $2.4 < \nu < 3.0$ mHz, as a function of spherical harmonic degree $\ell$. Note from these plots the apparent lack of any obvious solar cycle changes in linewidths.

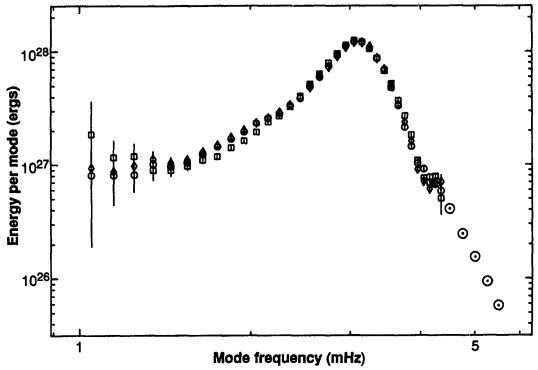


**Fig. 10.** Average energy per p-mode for low-$\ell$ modes, where the notation is the same as in Fig. 8. Here a solar model was used to generate p-mode masses, which with the amplitude measurements were used to estimate mode energies.

with $\ell$ out to $\ell \approx 200$, then decrease at still higher $\ell$; the mode linewidths almost certainly increase at higher $\ell$, but at present there are no accurate linewidth data at $\ell$ values above those shown in Fig. 9. Extrapolating the measured linewidths to higher $\ell$, we find that the linewidth $\Gamma > d\nu/d\ell$ for all modes with $\ell > 400$; thus for these larger $\ell$ values no p-modes are globally coherent.

Although the details of the excitation and damping mechanisms are still uncertain, it is clear that all these mechanisms operate very near the solar surface. For example, excitation of modes by the radiation field, the kappa mechanism, is occurring primarily in the hydrogen ionization zone, which is located a few scale heights below the photosphere. The competing process of radiative damping is significant near the photosphere but is negligible in the solar interior, because below the photosphere the time scale for photons to diffuse a distance of one oscillation wavelength is much greater than the period of the modes. Also, energy exchange with convection is greatest near the solar surface, because it depends strongly on the Mach number of the convective motion, which approaches unity near the photosphere and is small below.

This fact, that the excitation and damping processes all occur near the solar surface, qualitatively explains many of the observed trends in the mode properties. For example, for $\ell < 100$ the observed linewidths approximately separate into a function of frequency $\Gamma_0(\nu)$ times a weak function of $\ell$, as shown in Fig. 9. The constant frequency dependence results from the fact that at these $\ell$ values the eigenfunctions near the surface, the most important region, depend nearly exclusively on $\nu$, as discussed above, independent of $\ell$. The remaining $\ell$ dependence in the linewidth, approximately given by $M^{-1}(\ell)$, arises from the fact that modes with higher $\ell$ have higher surface amplitudes than lower $\ell$ modes (for fixed $\nu$ and mode energy). The lowest $\nu$ modes, which are trapped deepest below the surface, have the smallest linewidths, owing to their weaker interaction with the surface driving and damping forces.

The most important process responsible for the observed p-mode amplitudes appears to be stochastic excitation by turbulent convection (*24, 25*), first proposed for p-modes by Goldreich and Keeley over a decade ago (*26*) and recently refined by Goldreich and Kumar (*27, 28*). The basic idea is that turbulence in the sun's convection zone generates acoustic noise, and this acoustic noise trapped inside the sun excites the cavity's resonant modes, the p-modes. Recent calculations predict p-mode energies that are given by $E \simeq m\nu^2$, where $E$ is the energy per mode, $m$ is the mass of a resonant turbulent convective eddy, and $\nu$ is the convective velocity. In the photosphere a convective eddy is essentially a granulation cell, and we can write $E \simeq \rho HL^2\nu^2$, where $\rho \simeq 10^{-7}$ g/cm$^3$ is the density at $\tau_{5000}$ (optical depth at 5000 Å) = 1, $H \simeq 100$ km is the scale height, $L \simeq 1000$ km is the horizontal size of a granule, and $\nu \approx 0.1\ c \approx 1$ km/s, giving $E \sim 10^{26}$ ergs, not too far from the observations (Fig. 10). The turbulent excitation model not only predicts nearly the correct order of magnitude for the p-mode energies, but it also naturally explains the observation that millions of modes are simultaneously excited. However, a model reproducing the correct energy spectrum does not yet exist.

An interesting quantity to consider is the product of mode energy and linewidth as a function of frequency, $E\Gamma(\nu)$, for low-$\ell$ modes (*24*), because this is easier to describe theoretically. For a stochastically driven p-mode, $E\Gamma = \dot{E}$ is a measure of the power being pumped into the mode, presumably by convection. If one were to leave this input power fixed and arbitrarily increase, say, the radiative damping, then the mode energy would decrease and the linewidth would increase, but $E\Gamma$ would remain unchanged. The observations indicate that $E\Gamma \sim \nu^8$ for $\nu < 3$ mHz, $E\Gamma \sim \nu^{-5}$ for $\nu > 4$ mHz, and $E\Gamma \approx 10^{22}$ ergs/s at $\nu = 3.5$ mHz (*24*). Goldreich and Kumar (*28*) found that they can reproduce quite well the observed trends in $E\Gamma(\nu)$, both above and below the peak at $\nu \simeq 3.5$ mHz, supporting the hypothesis that p-modes are stochastically excited by turbulent convection. The observation of p-mode structure for $\nu > \nu_{a,\,max}$ also points toward turbulent convection as the most likely excitation mechanism (*29*).

## The Future

Work is under way on a new generation of helioseismology instruments that promise a tenfold or greater improvement in the accuracy of the measurements shown above. The Global Oscillation Network Group (GONG) (*30*), scheduled to begin operation in 1993, will consist of a network of six telescopes, spaced in longitude to provide continuous Doppler measurements of the solar surface for several years. Other networks of integrated sunlight instruments (*31*) will provide more accurate measurements of the properties of modes with $\ell \leq 3$. Meanwhile, the Solar Heliospheric Observatory (SOHO) spacecraft will contain several helioseismology instruments, including the GOLF (Global Oscillations at Low Frequencies) (*32*), and MDI (Michelson Doppler Imager) (*33*) instruments, which will provide precision measurements of low-frequency and high-$\ell$ oscillations, respectively.

These instruments, combined with theoretical advances yet to come, should provide an extremely detailed picture of many properties of the solar interior. Going beyond a basic understanding of the structure of the sun, these new helioseismological measurements are expected to turn the sun into a precision laboratory for learning about the physics of high-temperature plasmas and magnetohydrodynamics, neutrino oscillations, radiative transfer, and the dynamics of large-scale stratified convection and rotation.


REFERENCES AND NOTES

1. R. B. Leighton, R. W. Noyes, G. W. Simon, *Astrophys. J.* **135**, 474 (1962).
2. F.-L. Deubner, *Astron. Astrophys.* **44**, 371 (1975).
3. A. Claverie *et al.*, *Nature* **282**, 591 (1979); G. Grec, E. Fossat, M. Pomerantz, *ibid.* **288**, 541 (1980); *Solar Phys.* **82**, 55 (1983).
4. F.-L. Deubner and D. Gough, *Annu. Rev. Astron. Astrophys.* **22**, 593 (1984); J. Christensen-Dalsgaard, D. Gough, J. Toomre, *Science* **229**, 923 (1985); K. G. Libbrecht, *Space Sci. Rev.* **47**, 275 (1988); S. V. Vorontsov and V. N. Zharkov, *Sov. Sci. Rev. Sect. E Astrophys. Space Phys.* **7**, 1 (1989); H. Shibahashi, in *Progress of Seismology of the Sun and Stars*, Y. Osaki and H. Shibahashi, Eds. (Springer-Verlag, Berlin, 1990), p. 3.
5. P. Kumar and P. Goldreich, *Astrophys. J.* **342**, 558 (1989).
6. K. G. Libbrecht, M. F. Woodard, J. M. Kaufman, *Astrophys. J. Suppl. Ser.* **74**, 1129 (1990).
7. S. V. Vorontsov, V. A. Baturin, A. A. Pamyatnykh, *Nature* **349**, 49 (1991); other solar helium determinations are cited in this paper.
8. J. Christensen-Dalsgaard, in *Proceedings of the Symposium on the Seismology of the Sun and Sun-Like Stars*, E. J. Rolfe, Ed. [European Space Agency (ESA), Noordwijk, Netherlands, 1988], p. 431.
9. J. Christensen-Dalsgaard *et al.*, *Nature* **315**, 378 (1985).
10. H. Shibahashi and T. Sekii, in *Proceedings of the Symposium on the Seismology of the Sun and Sun-Like Stars*, E. J. Rolfe, Ed. (ESA, Noordwijk, Netherlands, 1988), p. 471.
11. S. V. Vorontsov, *ibid.*, p. 475.
12. Y. Elsworth *et al.*, *Nature* **347**, 536 (1990).
13. J. Christensen-Dalsgaard, D. O. Gough, M. J. Thompson, in preparation.
14. K. G. Libbrecht and M. F. Woodard, in preparation.
15. _____, *Nature* **345**, 779 (1990). Low $\ell$ results are also described on p. 768 of that issue.
16. K. G. Libbrecht and C. A. Morrow, in *The Solar Interior and Atmosphere* (Univ. of Arizona Press, Tucson, in press).
17. J. Christensen-Dalsgaard and J. Schou, in *Proceedings of the Symposium on the Seismology of the Sun and Sun-Like Stars*, E. J. Rolfe, Ed. (ESA, Noordwijk, Netherlands, 1988), p. 149.
18. G. A. Glatzmaier, in *The Internal Solar Angular Velocity*, B. R. Durney and S. Sofia, Eds. (Reidel, Dordrecht, 1987), p. 263; P. A. Gilman and J. Miller, *Astrophys. J. Suppl. Ser.* **61**, 585 (1986).
19. M. H. Pinsonneault *et al.*, *Astrophys. J.* **338**, 424 (1989).
20. H. C. Spruit, in *The Internal Solar Angular Velocity*, B. R. Durney and S. Sofia, Eds. (Reidel, Dordrecht, 1987), p. 185.
21. M. Woodard and R. W. Noyes, *Nature* **318**, 449 (1985).
22. P. Goldreich *et al.*, *Astrophys. J.*, in press.
23. J. Kaufman, thesis, California Institute of Technology (1990).
24. K. G. Libbrecht, in *Proceedings of the Symposium on the Seismology of the Sun and Sun-Like Stars*, E. J. Rolfe, Ed. (ESA, Noordwijk, Netherlands, 1988), p. 3.
25. Y. Osaki, *Progress of Seismology of the Sun and Stars*, Y. Osaki and H. Shibahashi, Eds. (Springer-Verlag, Berlin, 1990), p. 75.
26. P. Goldreich and D. A. Keeley, *Astrophys. J.* **211**, 934 (1977); *ibid.* **212**, 243 (1977).
27. P. Goldreich and P. Kumar, *ibid.* **326**, 462 (1988).
28. _____, *ibid.* **363**, 694 (1990).
29. P. Kumar and E. Lu, in preparation.
30. J. Harvey *et al.*, in *Proceedings of the Symposium on the Seismology of the Sun and Sun-Like Stars*, E. J. Rolfe, Ed. (ESA, Noordwijk, Netherlands, 1988), p. 203.
31. A. Aindow *et al.*, *ibid.*, p. 157; E. Fossat, *ibid.*, p. 161.
32. L. Dame, *ibid.*, p. 367.
33. P. H. Scherrer, J. T. Hoeksema, R. S. Bogart, *ibid.*, p. 375.
34. K. G. Libbrecht, *Astrophys. J.* **334**, 510 (1988).


35. We thank N. Murray and P. Goldreich for enlightening conversations. This work was supported by NSF grants ATM-8907012 and AST-8657393.


# Messenger RNA Splicing in Yeast: Clues to Why the Spliceosome Is a Ribonucleoprotein


CHRISTINE GUTHRIE



**The removal of introns from eukaryotic messenger RNA precursors shares mechanistic characteristics with the self-splicing of certain introns, prompting speculation that the catalytic reactions of nuclear pre–messenger RNA splicing are fundamentally RNA-based. The participation of five small nuclear RNAs (snRNAs) in splicing is now well documented. Genetic analysis in yeast has revealed the requirement, in addition, for several dozen proteins. Some of these are tightly bound to snRNAs to form small nuclear ribonucleoproteins (snRNPs); such proteins may promote interactions between snRNAs or between an snRNA and the intron. Other, non-snRNP proteins appear to associate transiently with the spliceosome. Some of these factors, which include RNA-dependent adenosine triphosphatases, may promote the accurate recognition of introns.**


LITTLE MORE THAN A DOZEN YEARS HAVE PASSED SINCE THE discovery of the "amazing" (*1*) process of RNA splicing. Although the removal of introns has already been comfortably assimilated into the canon of gene expression, the most basic questions about the molecular mechanisms of nuclear messenger RNA (mRNA) splicing remain unanswered. For example, we have only a limited understanding of how splice sites are chosen, and none as to how they are juxtaposed. Furthermore, the discovery of a class of self-splicing introns in organellar mRNAs has raised afundamental question. What catalyzes nuclear mRNA splicing: RNA, proteins, or a collaboration of the two? Here I review recent results from *Saccharomyces cerevisiae* that lend insight into why the spliceosome is made up of both RNA and protein. This yeast


The author is in the Department of Biochemistry and Biophysics, University of California, San Francisco, San Francisco, CA 94143.